Ordered Structure of Thermotropic Liquid-Crystal Polymers. 1. Characterization of Liquid-Crystal Domain Texture

Toshio Shiwaku,† Akemi Nakai, Hirokazu Hasegawa, and Takeji Hashimoto*

Department of Polymer Chemistry, Faculty of Engineering, Kyoto University, Kyoto 606, Japan. *Received July 27, 1989; Revised Manuscript Received October 5, 1989*

ABSTRACT: We investigated the growth and ordering mechanism of liquid-crystal texture in thin films of main-chain-type thermotropic liquid-crystalline copolyesters. The growth and ordering were induced by isothermal annealing of the film specimens, which were prepared by a solvent-cast method. The as-cast test specimens were isotropic, transparent, and homogeneous on a microscopic scale and in the glassy state at room temperature. The texture of the liquid crystals, which has an appearance of what is conventionally called the "domain texture" under optical microscopic observations, was found to originate from a spatial distribution of the disclinations with a strength of $\pm 1/2$ as the most popular type of disclination. The texture and its growth (domain growth) as a result of annihilation of the disclinations were investigated by light and electron microscopy as well as by light and X-ray small-angle scattering (SAXS) methods. We presented a model of the thermotropic liquid-crystal texture on the spatial scale of submicrometers to micrometers. The polymer in the nematic liquid-crystal state exhibits two-phase character, comprising regions rich in the mesogenic units and those rich in the flexible spacer units, at a spatial scale of a few tens of nanometers under SAXS examination even when the specimens become completely anisotropic under optical microscopic observation.

I. Introduction

Since the success in preparing main-chain-type thermotropic liquid-crystalline copolyesters,[1,2] there have been a number of works reported on rheological properties;[1-5] the strength, modulus, and flow properties; supermolecular structures[6-15] as a function of temperature; and phase transition[16-20] of crystalline state, liquid-crystal state, and isotropic liquid state.

The copolyesters comprised of *p*-hydroxybenzoic acid (OBA) and ethylene terephthalate units (PET) with a 60/40 mol/mol composition (such as X-7G provided by Tennessee Eastman Co.) that we studied here have a high phase-transition temperature T_{NI} at which the nematic liquid-crystal phase is completely transformed into an isotropic phase. At temperatures $T > T_{NI}$, the polymers are usually chemically unstable. This situation makes it difficult to erase completely the thermal history built in the as-polymerized samples. Most of the works that have been performed under such constraints hence suffer from the memory effects and lack universality to a certain extent.

In order to circumvent the disadvantage described above, we completely erased the structure memory that existed in the as-polymerized specimens by dissolving as-polymerized samples in a solvent.[15,21] Thin films about 10 μm thick were prepared by a rapid solvent-casting method.[15,21] The film specimens prepared and used as starting samples in our work were transparent, optically isotropic, and homogeneous under optical microscopic observations. We then imposed temperature jumps to the starting thin film specimens and conducted real-time and in-situ investigations of the ordering process from the glassy amorphous state to the liquid-crystal state. The domain growth or coarsening of the Schlieren texture of the liquid crystals was investigated by optical microscopy, light scattering, small-angle X-ray scattering (SAXS), and wide-angle X-ray diffraction (WAXD). The electron microscopic (EM) investigations were also done.

† Present address: Polyplastics Co., Ltd., Research Center, 973 Miyajima, Fuji-city, Shizuoka-Pref. 416, Japan.

II. Experimental Methods

The material used in this study was a copolyester of 60 mol % *p*-oxybenzoate (OBA) and 40 mol % ethylene terephthalate (X-7G, Tennessee Eastman Co.), which is the main-chain thermotropic liquid-crystalline polymer. The as-received material in the form of pellets was dissolved in *o*-chlorophenol (ca. 1–2 wt % polymer) at 60 °C. The solution was turbid at this point due to the existence of small amount (less than 1 wt %) of insoluble particles, which were considered to consist of copolymers rich in OBA component and to be highly crystalline. In order to remove the insoluble material, the solution was filtered first through filter paper and subsequently through a Millipore membrane with the pore size of 0.5 μm. Then the solution became clear. One or two drops of the solution was poured onto a microscope cover glass, and the solvent was rapidly evaporated in a vacuum oven controlled at 60 °C, the solvent evaporation taking place within a few minutes. The as-cast thin films of a few micrometers thickness were further dried under vacuum before they were used for the temperature-jump (T-jump) experiments.

The as-cast films thus prepared were transparent, optically isotropic, and homogeneous on optical microscopic examination. In this way the starting film specimens were forced to be locked in the amorphous glassy state. The test specimens, i.e., the as-cast films with a microscope cover glass only on one side, were then subjected to T-jumps to various temperatures by placing them on a heating stage (TH-600 Type, LINKAM Scientific Co.) controlled at a preset temperature. The test specimens reached the preset temperature within a few seconds. The ordering process of the thin films of X-7G occurring during the isothermal annealing were investigated by real-time and in-situ observations under a light microscope (Nikon Optiphot-Pol XTP-11) and by a laser light scattering method.

The crystallinity and fine structure of the as-received (as-polymerized) specimens were also studied in situ as a function of temperature by WAXD and SAXS. For this purpose we used the apparatus consisting of a 12-kW rotating-anode X-ray generator (Rigaku Ru-a operated at 50 kV and 200 mA), a graphite monochromator (Cu Kα line being used), and a position-sensitive detector. The details of the apparatus have been described elsewhere.[22] The SAXS profiles were corrected for the slit height and width smearings and for absorption when necessary.[23]

Transmission electron microscopic observation was performed on ultrathin films of X-7G cast from a 1.0% solution in

0024-9297/90/2223-1590$02.50/0

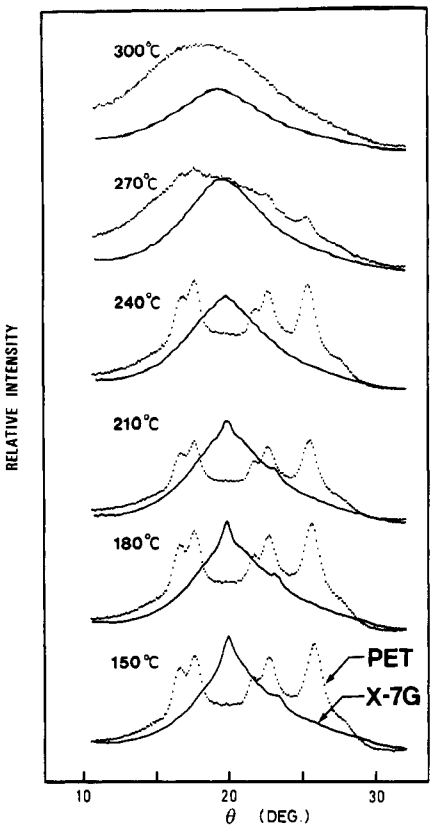

Figure 1. Comparison of wide-angle X-ray diffraction profiles obtained from X-7G (solid curves) and PET (dotted curves) at 150, 180, 210, 240, 270, and 300 °C.

o-chlorophenol on the surface of distilled water and subsequently picked up on microscope grids coated with a carbon supporting film. This film was also optically isotropic and homogeneous under a light microscopic observation. The ultrathin films were heat treated under various conditions on the same heating stage used for the light microscopy and observed without staining or shadowing under a Hitachi H-600 electron microscope. The phase contrast technique[24] (defocusing technique) was used to obtain the contrast to form the images.

III. Experimental Results

1. **WAXD.** The WAXD profiles were taken as a function of temperature. For the WAXD studies, the solvent-cast films as described in section II were not used, simply because they are too thin. Instead we used the isotropic X-7G sample prepared by annealing the as-received pellets at 260 °C for about 10 h in an X-ray sample holder under an N_2 atmosphere, followed by slow cooling to room temperature. The orientation existing in the as-received pellets became random by the annealing process in the sample holder. The PET specimen was mounted in the X-ray sample holder after drying under vacuum at 60 °C for 24 h. The WAXD profiles for X-7G and PET were measured at each temperature by elevating the temperature stepwise in order to measure the melting temperatures. Figure 1 shows the typical diffraction profiles for X-7G and poly(ethylene terephthalate) (PET).

As compared with the diffraction profiles of the pure PET specimen, those of X-7G did not exhibit the diffraction peaks relevant to its PET sequences but the sharp diffraction peak at scattering angle $\theta = 19.7°$ (Bragg spacing $d_{Bragg} = 0.45$ nm) due to its OBA sequences.[7,11,25] The subsidiary peak at $\theta = 23.1°$ ($d_{Bragg} = 0.38$ nm) may be also due to the intramolecular atomic order of OBA sequences as previously discussed by other investigators.[8,11] From the figure the melting of X-7G was observed to occur at 210 °C < T < 240 °C, the detailed examination showed that the melting temperature is approximately 233 °C, at which the diffraction peak of the OBA crystals at $\theta \cong 20°$ completely disappears. Hereafter we define this melting temperature as $T_{m,OBA}$. T_m for PET is about 275 °C. Information obtained by WAXD studies is important to understand SAXS and EM results as will be discussed later.

2. **Formation and Growth of Domains in the Liquid-Crystal State.** Here we report our experimental results on the ordering process of X-7G from the amorphous glassy state to the liquid-crystal state, which is induced by isothermal heat treatments at temperatures above T_g of X-7G. In order to understand qualitatively the overall trend of the ordering process, it is useful to observe the formation of the texture during the heating process from room temperature to 430 °C at a constant rate. Figure 2 shows an example of such an investigation at 10 °C/min with crossed polarizers and a red retardation plate. The micrograph for the as-cast film is red and shows no significant structure, implying that the as-cast film is optically isotropic and homogeneous at the spatial scale of the observation. At temperatures below 120 °C, no significant structure appears, and at T > 120 °C, weak optical anisotropy gradually starts to appear. The micrograph at 150 °C represents the typical structure in the temperature range 120 °C < T < 180 °C. This result qualitatively implies that T_g of the as-cast thin film is approximately 120 °C. This temperature is different from T_g of X-7G reported by Menczel and Wunderlich[17] (57–67 °C and 152–197 °C) or by Viney and Windle[19] (70 °C) from DSC measurements. This is because our starting test specimen was in the amorphous homogeneous glassy state while their samples were as received and in the state of a frozen-in liquid crystal. In fact DSC measurement of our as-cast films showed the endothermic change at ca. 120 °C, but it was not observed in the second heating cycle.

At higher temperatures what is called the domain texture with retardation colors relevant to the liquid-crystal state appears as typically shown in the micrographs obtained at $T \gtrsim 200$ °C. However, at 120 °C $\lesssim T \lesssim$ 230 °C, the size of the domains does not increase beyond a certain limit. This may be a consequence of the crystallization of X-7G pinning the growth of the domain, because it suppresses the large-distance-scale translational diffusion of X-7G molecules. The domain can grow effectively until sufficient crystallinity develops. At $T \gtrsim 230$ °C, the domains tend to grow into bigger sizes as shown by the micrographs at 250 and 290 °C.

At $T \gtrsim 290$ °C, the area fraction showing optical anisotropy decreases with increasing temperature as shown by the micrographs for 400 °C and completely disappears at T > 400 °C as shown by the micrograph at 420 °C. This observation indicates that the nematic-to-isotropic transition takes place over a wide temperature range for this specimen as previously reported.[19] The micrograph at 400 °C shows a biphasic nature, showing a coexistence of anisotropic and isotropic phases. The specimen was substantially degraded thermally, and hence the same domain structures as observed in the heating cycle were not recovered upon lowering the temperature from 420 °C.

Figure 3 shows the time evolution of the liquid-crystal texture during the ordering process induced by the T-jump at 260 °C, where the micrographs were taken in situ with crossed polarizers and without a retardation

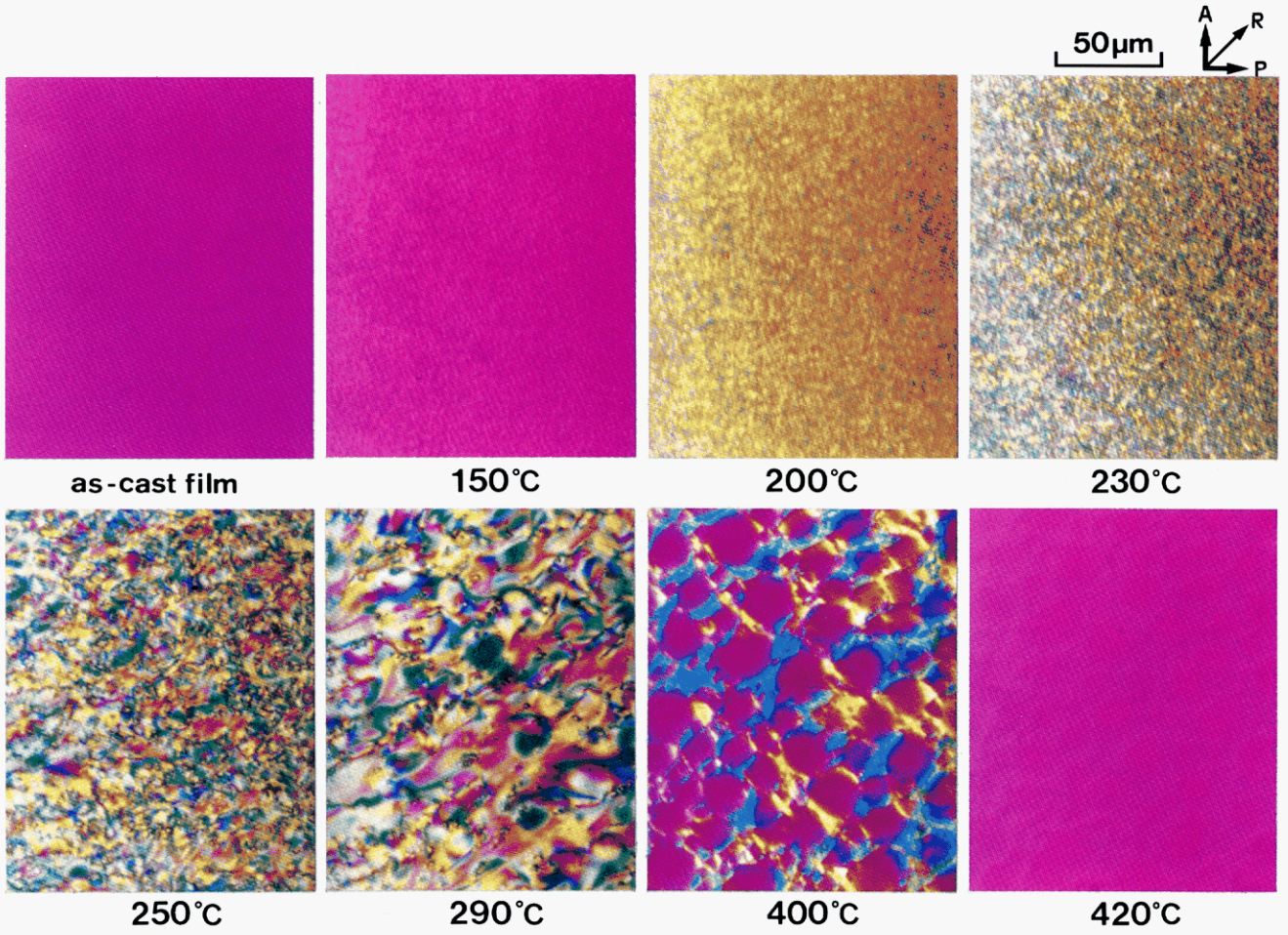

Figure 2. Light micrographs of an X-7G thin film observed in situ during a heating process at a rate of 10 °C/min between crossed polarizers and with a red (530 nm) retardation plate. The polarizer and analyzer were set in horizontal and vertical directions.

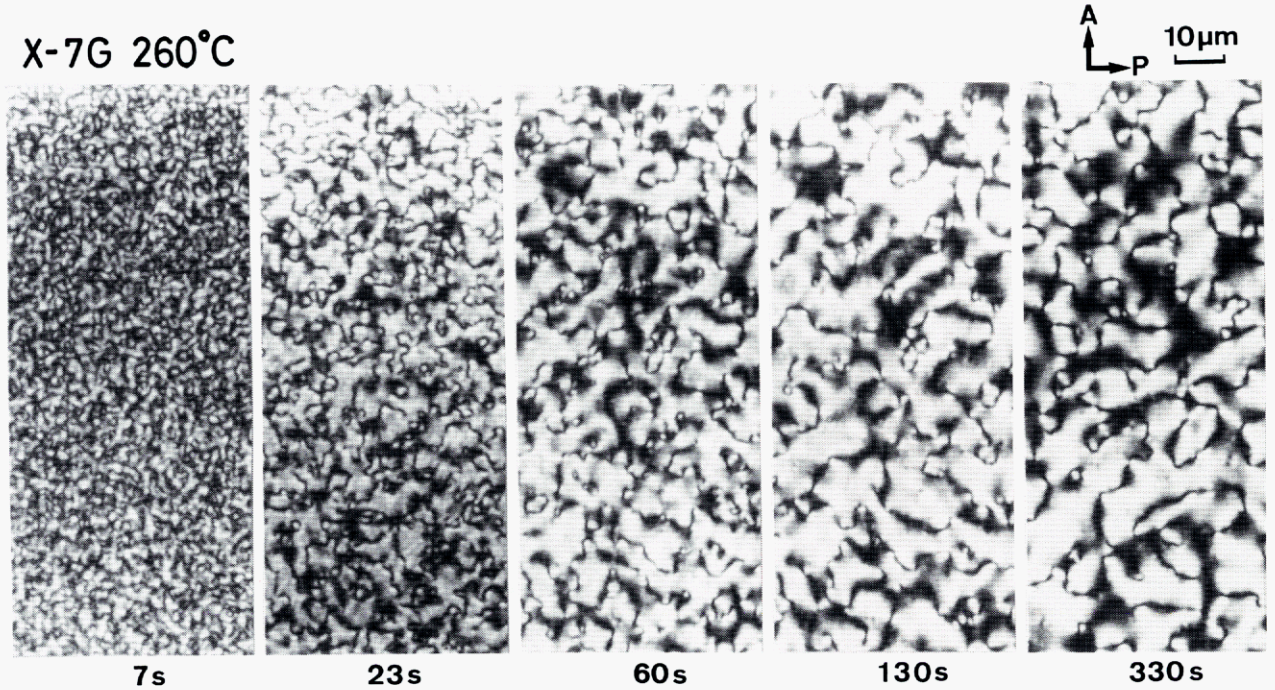

Figure 3. Polarized light micrographs of an X-7G thin film observed in situ during an isothermal annealing process at 260 °C. Continuous growth of Schlieren texture is seen.

plate. The optical anisotropy of the liquid-crystal phase appears quite rapidly, almost instantaneously, and uniformly over the sample space. This implies that the transformation of the specimens from the amorphous and glassy state to the liquid-crystal state occurs almost instantaneously at these temperatures. The same tendency was observed in the ordering processes at $T \gtrsim 120$ °C. During the annealing process the liquid-crystal texture and

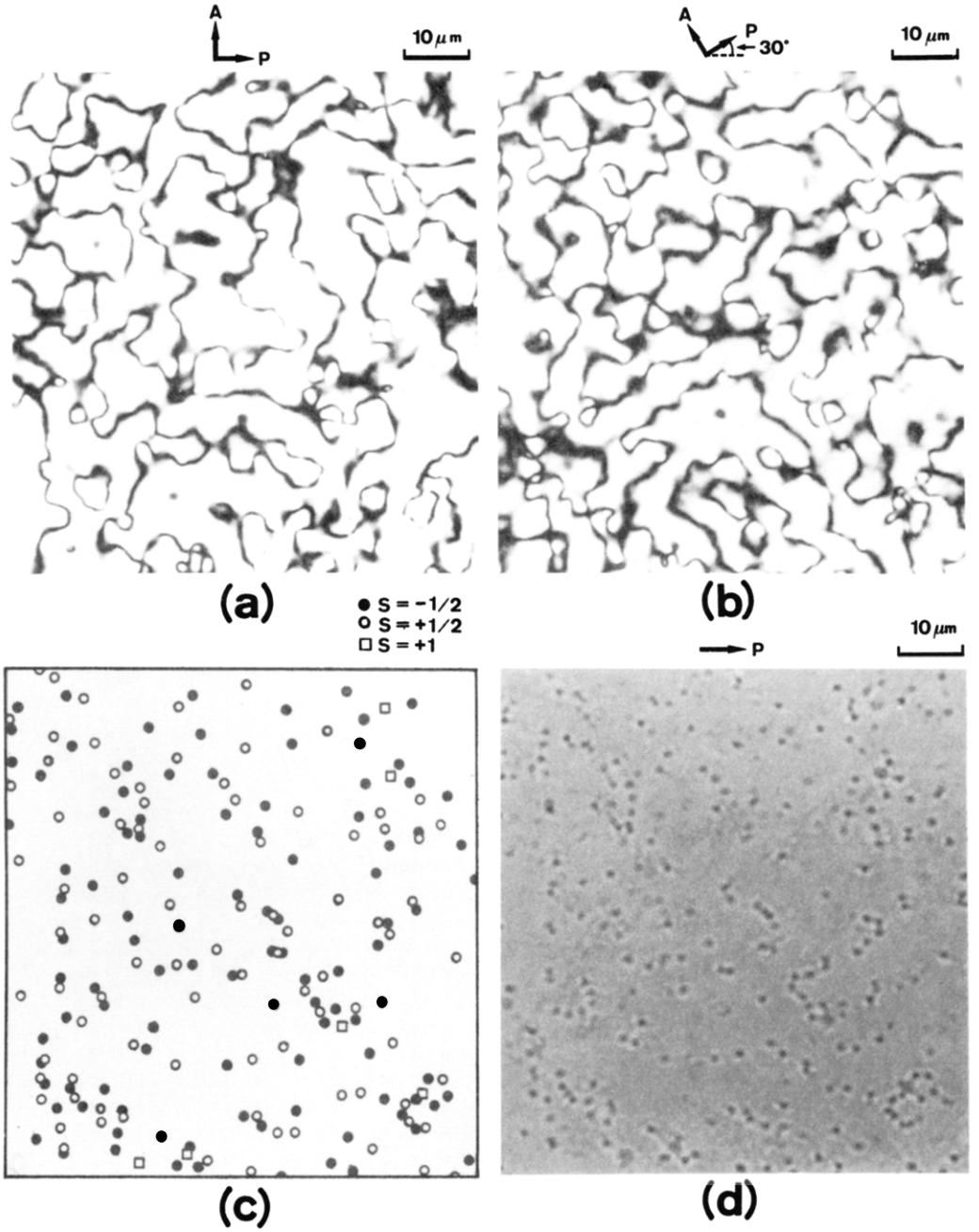

Figure 4. (a) Polarized light micrograph of an X-7G thin film annealed at 270 °C for 60 s and quenched to room temperature. The polarizer and analyzer were set in horizontal and vertical directions, respectively. (b) The same area as (a) but the crossed polarizers were rotated by 30° counterclockwise from the direction used in (a). (c) Location and strength of disclination lines corresponding to the Schlieren texture in (a) and (b): (●) $S = -1/2$; (○) $S = +1/2$; (□) $S = +1$. (d) The same area as (a) and (b) observed without an analyzer, showing dark spots that superpose on the disclination lines marked in (c).

the domains grew with time. However, at $T < T_{m,OBA}$, the domain growth was pinned at a certain spatial scale, and no further growth of the domain was observed beyond a certain annealing time. The pinning of the domain growth is believed to result from the increasing amount of the crystallinity of X-7G or more specifically the crystallinity of the OBA units with time, which hinders or suppresses the large spatial-scale translational diffusion of the molecules required for the domain growth. Here the domain growth occurs before a sufficient amount of the crystallinity of the X-7G appears. At $T = 260$ °C > $T_{m,OBA}$ the domains continue to grow as shown in the figure, and no pinning due to the crystallization of X-7G was observed. The higher the annealing temperature was, the faster the domains were observed to grow, simply reflecting larger mobility at higher temperatures.

Parts a and b of Figure 4 show a close-up of the domain structure observed between crossed polarizers after 60 s from the T-jump to 270 °C. Part a was obtained with the polarizer and analyzer in horizontal and vertical orientation, respectively, and part b was obtained by rotating both of them by 30° counterclockwise. These micrographs were obtained on the specimen quenched to room temperature, but we confirmed that there was no significant change before and after the quench. Therefore, these micrographs represent the close-ups of the domain structures shown in Figure 3. It clearly shows that the domain textures observed in Figure 3 and parts a and b of Figure 4 originate from the Schlieren texture. The dark brushes correspond to the regions having the extinction condition between the crossed polarizers where the directors orient either parallel or perpendicular to the elec-

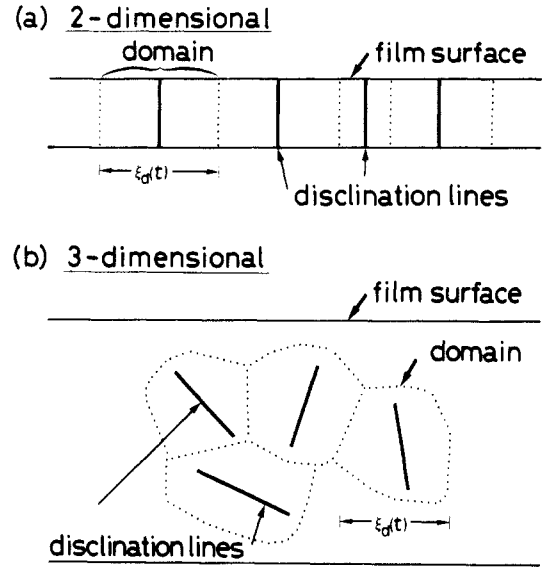

Figure 5. Schematic diagrams of liquid-crystal "domains" and disclination lines. Disclination lines and domain boundaries are indicated by thick solid and thin broken lines, respectively, although there exist no domain walls. (a) Two-dimensional case. Disclination lines and domain boundaries are normal to the film surface. (b) Three-dimensional case. Disclination lines are randomly oriented with respect to the film surface.

tric vector of the polarizer or analyzer. The domain texture, i.e., the pattern resulting from the dark brushes, reflects a spatial distribution of the disclination lines oriented essentially normal to the film surfaces of the thin-film specimens in this case.[15]

The strength $|S|$ and sign of the disclinations were analyzed by a conventional method[26,27] on the quenched specimen, i.e., by observing a number of dark brushes emanating from the disclination lines and by observing the sense of the rotation of the brushes accompanied by the rotation of the crossed polarizers as shown in parts a and b of Figure 4. The spatial distribution of the disclinations and their strength and sign for the pattern shown in Figure 4a were identified in Figure 4c. The pattern in part d was obtained with only a polarizer and no analyzer, and the dark spots show the spatial distribution of disclinations as will be discussed more in depth in section III-3. The parts a to d of Figure 4 correspond to the same area so that they should superimpose for a better understanding of the pattern.

The results shown in Figure 4c clearly show that a majority of the disclinations have strength $S = \pm 1/2$ and only a few have $S = \pm 1$, which is quite reasonable since the free energy of the disclinations is proportional to $|S|^2$ as predicted by the continuum theory of Frank.[26]

3. Nature of the Domains and Mechanism of Domain Growth. The orientation of the directors changes about the disclination lines in a manner determined by their sign and strength. Thus the overall texture of the liquid crystal is determined by the spatial distribution of the disclination lines. The disclinations cause continuous changes of the director orientations as will be shown later in Figures 8 and 9. Their spatial distribution determines the orientation correlation of the directors. Thus as schematically shown in Figure 5, the net volume of the liquid crystal can be divided into subvolumes, each of which contains a single disclination line. We define the domains as such subvolumes, within which the directors undergo a characteristic change in orientation (see Figures 8, 9, and 14).[28,29] Therefore, the average domain size is closely related to the number density and the spatial distributions of the disclinations. The director orientation is continuous at the domain boundary. There is no evidences for domain walls where the director orientation becomes discontinuous as inferred by some previous reports.[30] In thicker films, disclination lines may be oriented randomly in three-dimensional space (as schematically shown in part b of Figure 5), contrary to the case of the thin films (part a of Figure 5) as we found in our experiments.

Since disclinations are line defects, they contain excess free energy. This excess free energy is relaxed during the ordering process that is induced by the isothermal heat treatments at $T > T_g$. This ordering process involves a decrease in the number density of disclination lines, $\rho(t)$, and an increase in the domain size, $\xi_d(t)$, by annihilation of the disclination lines, which in turn occurs as a consequence of the diffusion and coalescence of the disclination lines of opposite signs ($S = \pm 1/2$). The two quantities ξ_d and ρ are obviously interrelated

$$\xi_d(t) \sim \rho(t)^{-1/d} \tag{1}$$

where d is a spatial dimensionality and the measurement of one of the quantities as a function of time is crucial to understand the ordering process and dynamics.

We report here a quick method that enables us to determine the spatial distribution of the disclination lines during the ordering process and hence to investigate the dynamics of the domain growth, $\xi_d(t)$. This method was developed by utilizing earlier findings by Friedel[31] and by others[6,32] that the disclinations appear as dark filaments under a light microscope with unpolarized illumination. The dark appearance was proposed to be due to the refraction effects caused by the sudden changes in refractive index. Figure 4d illustrates the principle of this method, where light micrographs (part a, b, and d) were taken at the same sample area.

The Schlieren texture shown in Figure 4a,b under crossed polarizers changes to the pattern comprising the dark spots shown in Figure 4d when one or both of the polarizers are removed from the microscope. The symbols shown in Figure 4c represent the locations of the disclinations, which were identified from the Schlieren texture shown in parts a and b. It should be noted that the dark spots shown in Figure 4d, except for a few minor spots, overlap the disclinations identified in Figure 4c and hence those in Figure 4a,b. This result implies one-to-one correspondence of the dark spots and the disclination lines that are located at the intersections of the dark brushes. Our interpretation of this effect is as follows; in our thin specimen, the disclination lines are normal to the film surface, and hence they appear as dark spots under unpolarized illumination, whereas the former observations of the dark filaments[6,31,32] were made on the disclinations more or less parallel to the film surfaces.

We proposed[15] that the strong scattering from the disclination lines reduces the transmitted light intensity along the lines and hence makes the lines appear dark. The strong scattering from the disclination lines is due to the singularity of the disclination lines in terms of orientation of the director. This idea may be confirmed by a dark-field light micrograph as typically shown in Figure 6 where the disclination lines appear bright in the dark-field image (part b), indicating that the scattering is a primary cause of the dark appearance in the bright-field image (part a). It should be noted that the dark spots in part a overlap the bright spots in part b but not vice

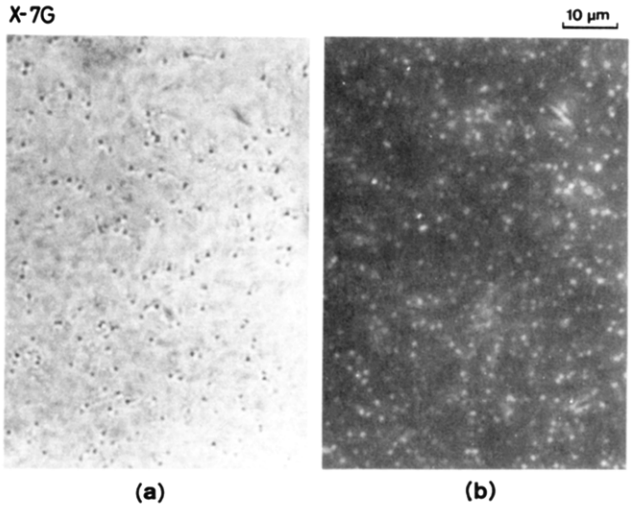

Figure 6. Unpolarized light micrographs obtained from an X-7G thin film annealed at 270 °C for 600 s and quenched to room temperature: (a) bright-field image; (b) dark-field image. Dark spots in (a) superpose on the white spots in (b).

versa. More bright spots are observed in part b than the dark spots in part a. The origin of the extra bright spots in the dark-field micrographs is not clear. It could be the residual strain or small crystallites in the quenched specimens. The number of the dark spots in the bright-field micrographs is not sensitive to the observation conditions such as the magnification of the objective lens or the size of the aperture. However, the number of the bright spots and their brightness strongly depend on the range of scattering angle in which scattered light is collected to form the image. The extra bright spots are sometimes much brighter than those corresponding to the disclination lines. Therefore, the dark-field micrographs cannot be used to determine the disclination lines unequivocally.

In Figure 4 the following unique points should be noted: (i) the disclinations of $S = +1$ were found but no disclination with the opposite sign ($S = -1$) were found, (ii) the dark spots corresponding to $S = +1$ appear different from those corresponding to $S = \pm 1/2$ (the former image being bigger and more diffused than the latter images (Figure 4d), (iii) the disclinations of $S = +1$ are surrounded by those of $S = -1/2$, and (iv) alternating chain sequences of $S = +1/2$ and $-1/2$ are observed along the dark brushes in the Schlieren texture.

During the isothermal annealing process at 240 °C, the number density of disclination lines $\rho(t)$ was observed in situ between the crossed polarizers and also with unpolarized light. The coarsening of the Schlieren texture with t was observed between the crossed polarizers, and the decrease of $\rho(t)$ with t was observed by unpolarized light microscopy. Both results are indicative of the domain growth as a consequence of annihilation of disclinations. The domain growth $\xi_d(t)$ during the ordering process involving the free energy relaxation was estimated from the measurements of $\rho(t)$ by unpolarized light microscopy, the result of which gave

$$\xi_d(t) \sim \rho(t)^{-1/2} \sim t^{0.35} \tag{2}$$

at 240 °C.

4. Characterization of the Domain by SALS. The domain growth during the ordering process after a T-jump can be investigated by depolarized (H_V in Figure 7a) and polarized (V_V in Figure 7b) components of small-angle light scattering (SALS) obtained from the quenched

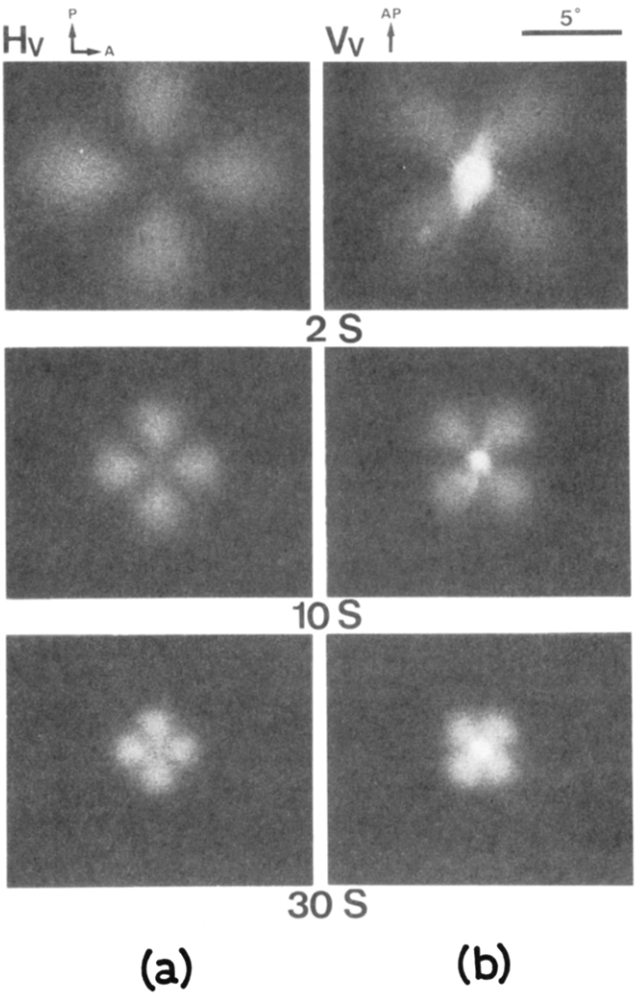

Figure 7. Small-angle light scattering patterns obtained from X-7G thin films annealed at 240 °C for 2, 10, and 30 s and quenched to room temperature: (a) H_V; (b) V_V.

specimens. The SALS was shown to depend on spatial orientation fluctuation and its correlation of the directors, which in turn depends on $\xi_d(t)$ and $\rho(t)$. Many-body interactions of the disclinations were proposed to be an origin of the scattering maxima qualitatively by Hashimoto et al.[33] and more quantitatively by Greco.[34] Figure 7 typically represents change of the SALS with time after the T-jump to 240 °C. The result clearly indicates that the scattering angle θ_{max} of the maximum intensity for H_V scattering is identical with that for V_V scattering and it shifts toward a smaller angle during the ordering process. The magnitude of the scattering vector q_{max} corresponding to θ_{max} is related to ξ_d

$$\xi_d(t) \sim 2\pi/q_{max}(t) \tag{3}$$

$$q_{max}(t) = (4\pi/\lambda) \sin(\theta_{max}(t)/2) \tag{4}$$

where λ is the wavelength of light in the medium. Thus the shift of the θ_{max} or q_{max} is a consequence of the growth of $\xi_d(t)$. This method also yielded the same scaling relation as given by eq 2.

5. Characterization by Electron Microscopy. Figure 8 shows a transmission electron micrograph on the ultrathin film annealed at 180 °C for 10 s and subsequently cooled to room temperature slowly on the microscope grid. The micrograph shows fine striations reminiscent to the director trajectories about the disclination lines of strength $S = \pm 1/2$. Some of the disclinations are identified on the micrograph, and Figure 9 shows a sketch of the fine striations and locations of the discli-

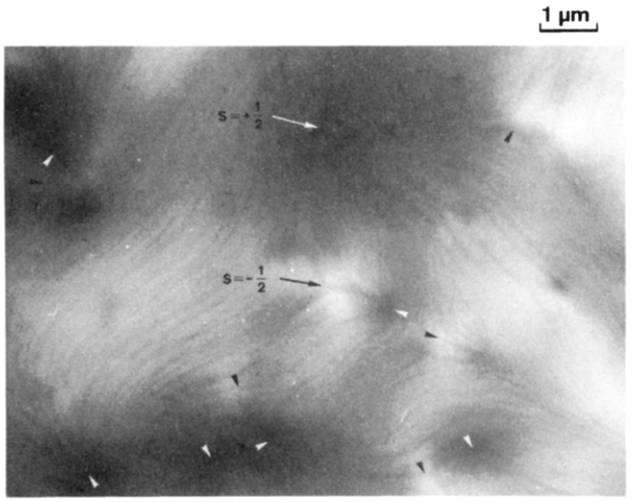

Figure 8. Phase-contrast (defocussed) electron micrograph obtained from an X-7G ultrathin film annealed and slowly cooled on a carbon-coated grid. Dark striations imply disclinations of $S = \pm 1/2$. Disclinations with $S = -1/2$ are indicated by dark arrows and those with $S = +1/2$ by white arrows.

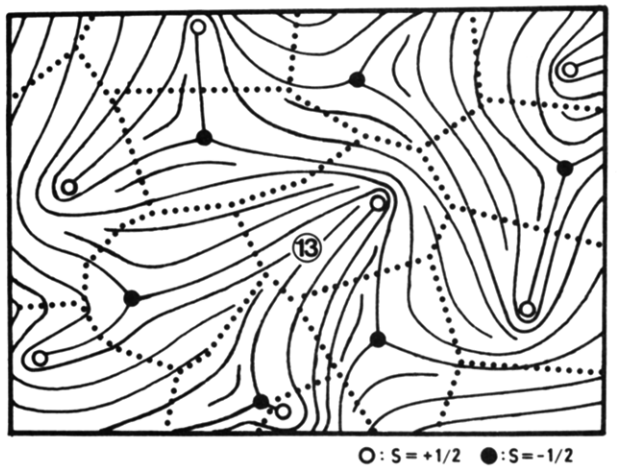

Figure 9. Schematic representation of the polydomain structure of X-7G produced by spatial distribution of disclination lines of $S = +1/2$ (open circle) and $S = -1/2$ (filled circle) based on the electron micrograph in Figure 8.

nation lines of $S = \pm 1/2$ corresponding to the striations. The fine striations are believed to originate from a phase contrast between the regions of higher and lower crystallinity or those of higher and lower density. Hence these striations correspond to those formed by "lamellar decoration" as reported by Thomas and Wood[24] and certainly reflect orientation of the directors. Unlike their polymer sample, X-7G did not have enough crystallinity for us to observe the electron diffraction patterns or the dark-field images. The contrast was obtained only under the defocusing condition with the bright field mode. As will be discussed later, these striations are expected to be perpendicular to the director but not to be parallel to the director. These striations suffice to demonstrate how the directors continuously change their orientation according to the spatial distribution of the disclination lines. Figure 9 also shows schematically the domains with an average size $\xi_d(t)$, i.e., the subvolumes divided by the disclinations. It should be noted that this model does not impose discontinuity of the director orientation at the domain boundary. The domains have the statistical property that characterizes the spatial scale of the orientational fluctuations. The fine structure existing in the vicinity of area numbered thirteen will be discussed later in conjunction with Figure 14.

6. Characterization by SAXS. Up to this point the domain texture was investigated mostly on the microscopic scale, except for the investigation by electron microscopy (Figures 8 and 9). Here we investigate the liquid-crystal texture on the spatial scale of a few tens of nanometers using small-angle X-ray scattering (SAXS).

Figure 10 shows SAXS scattering profiles measured in situ at each temperature for X-7G (a) and PET (b), where θ is the scattering angle. The profiles were normalized for sample thickness and exposure time and corrected for air scattering and absorption but were not corrected for slit smearings. Therefore, the intensity levels of the scattering profiles can be compared each other although only the relative intensity data are shown. The profiles were measured on the specimens subjected to the following thermal history: The test specimen of X-7G was obtained by casting from a 5 wt % *o*-chlorophenol solution in a Petri dish placed in a vacuum oven at 60 °C. The obtained cast film was much thicker than those used for optical microscopy, and they already possessed the optical anisotropy due to the nematic liquid-crystal phase and crystallites because of the slow solvent evaporation process. The test specimen of X-7G, a pile of the cast films, was first measured at room temperature (30 °C) and subsequently at 160, 180, 200, 220, 240, 260, 280, and 300 °C. The specimen was held at these temperatures for 0.5 h before each measurement, the exposure time of which was 5 h each. SAXS measurements of PET were performed at 255, 265, and 275 °C on the as-received pellets, which were dried under vacuum for 2 days and trimmed to fit in the X-ray sample holder. Time of preheating and measurement for PET was 0.25–1.5 and 1–4 h, respectively.

The broad peak at $\theta = 30$ min observed for the PET specimen at 255 °C is due to the long spacing of the lamellar crystallites of PET. The peak shifts toward smaller θ with the temperature raised to 265 °C, as a consequence of an expansion of interlamellar spacing, which, in turn, is induced by the lamellar thickening. Upon melting, however, the peak disappears, and the intensity is suppressed to the level relevant to the thermal diffuse scattering (TDS)[39] as shown typically by the profile obtained at 275 °C, i.e., the intensity is nearly independent of θ.

The scattering profiles for X-7G (Figure 10a) are considerably different from those of PET: the intenstiy level of X-7G at $\theta > 15$ min is much lower than that of PET, and hence the intensity reaches the TDS level at much lower scattering angles, i.e., at $\theta > 105$ min for the X-7G profiles compared with the PET profiles, which attain the TDS intensity level at $\theta > 150$ min. At $T \lesssim 230$ °C, the X-7G specimen has crystallinity resulting primarily from the OBA crystals, so that the profiles at 30 and 160 °C essentially reflect a two-phase state, comprising crystalline and amorphous regions or high- and low-density regions.

It should be noted, however, that a remarkable intensity excess to the TDS level still exists even above the melting temperature of X-7G ($T_{m,X\text{-}7G} = T_{m,OBA} = 233$ °C) as seen in the profile measured at 260 °C, whereas the intensity goes down to the TDS level at temperatures above the melting point in the case of the PET specimens as discussed above (the profile at 275 °C). This gives a very important conclusion that the two-phase nature exists even above $T_{m,X\text{-}7G}$ and in the temperature range where the specimens are completely and uniformly in the

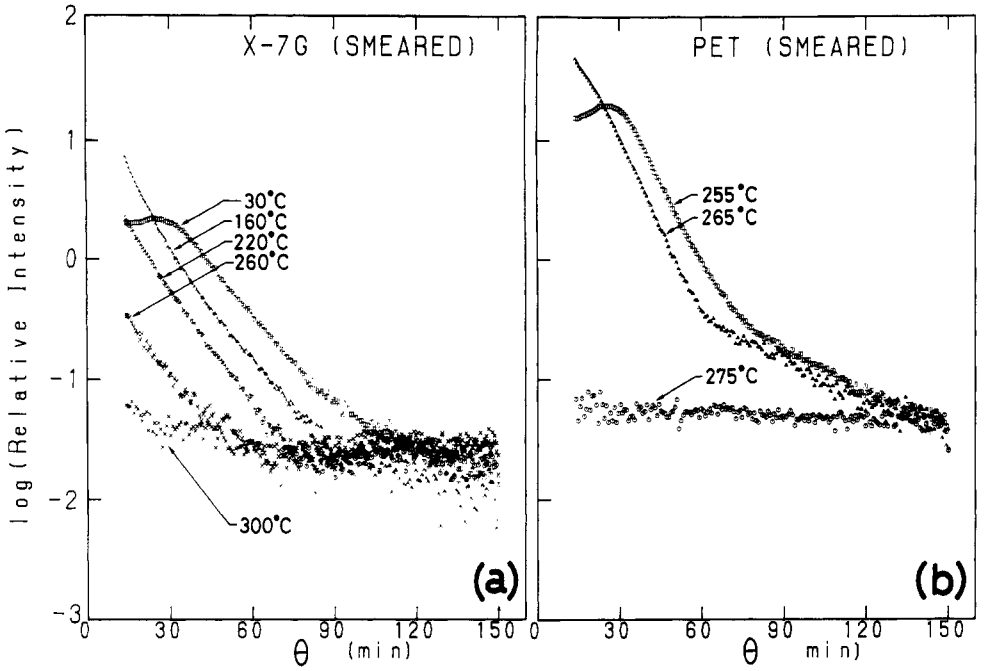

Figure 10. Small-angle X-ray scattering profiles obtained at various temperatures for (a) X-7G and (b) PET.

liquid-crystal state on the optical microscopic scale, although the electron density fluctuations decrease as the temperature is raised. The spatial scale of the density fluctuations is in the range of 20–40 nm and is believed to reflect the regions rich in the PET sequences and the OBA sequences (see Figure 14). At 300 °C, the scattering from the density fluctuations further decreases so that the TDS level appears to dominate at $\theta > 30$ min.

Since up to 290 °C we do not observe the existence of the biphasic structure comprising anisotropic and isotropic regions on the microscopic scale, the excess scattering at 233 °C $\lesssim T <$ 290 °C is believed to arise from the two-phase structure existing on a few tens of nanometers scale. At temperatures higher than 290 °C, we observe the biphasic structure in the microscopic scale.

The short-distance-scale density or composition fluctuation existing in the uniformly anisotropic liquid-crystal phase under microscopic observation is expected to be preserved below $T_{m,X\text{-}7G}$. The crystallinity of X-7G below $T_{m,X\text{-}7G}$ enhances the phase contrast under TEM observations. The enhanced phase contrast due to the crystallinity of the OBA sequences is believed to result in the striations in TEM observations (as shown in Figure 8), which dictate the orientation of the directors existing in the liquid crystals ("lamellar decoration"[24]). In order to carry out an order estimation of the spatial scale of the density fluctuations, we assume that the excess scattering in the uniformly anisotropic liquid-crystal phase is described by the Debye's scattering for the ideal two-phase structure:[35]

$$I(s) = \frac{I(0)}{[1 + (2\pi s)^2\xi^2]^2} \tag{5}$$

where s is the magnitude of the scattering vector defined by

$$s = (2/\lambda) \sin (\theta/2)$$

λ being the wavelength of the X-rays (λ = 0.154 nm) and θ being the scattering angle. $I(0)$ is the scattering intensity at $s = 0$, and ξ is the correlation length for the density fluctuations. $I(s)$ is the scattering intensity excess to the thermal density fluctuations, which is defined as

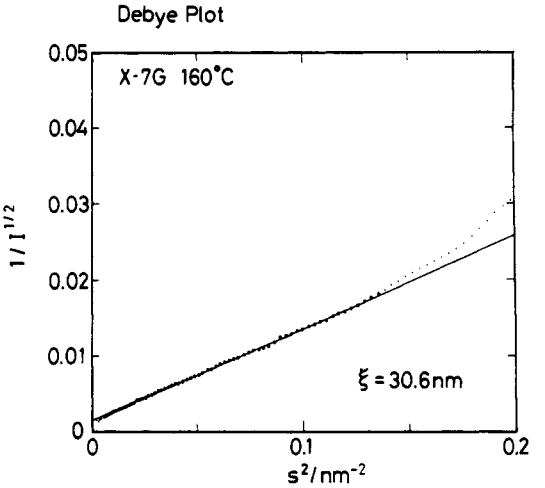

Figure 11. Example of a Debye plot ($I^{-1/2}$ versus s^2) for the small-angle X-ray scattering from X-7G (at 160 °C).

I_b below and which is approximately independent of θ. Figure 11 shows a typical Debye plot for the X-7G specimen at 160 °C after corrections for the slit smearings. At $s^2 \lesssim 0.15$ nm^{-2}, the intensity distribution is obeyed by the Debye formula, and the plot gave the value ξ = 31 nm.

Upward deviation of the data points from the straight line in the Debye plot may be due to the effect of the diffuse boundary between the two coexisting phases. If the electron density profile across the interface of the two phases is given by[36-38]

$$\rho_{el}(x) = \rho^{\circ}_{el}(x) * h(x) \tag{6}$$

$$h(x) \sim \exp(-x^2/2\sigma^2) \tag{7}$$

where $\rho^{\circ}_{el}(x)$ is the electron density profile having a sharp interface (i.e., for the ideal two phase), which gives rise to the scattering given by eq 5, σ in $h(x)$ is the parameter characterizing the interfacial thickness, and the asterisk (*) designates a convolution product. The scattering intensity function $\tilde{I}(s)$ for the pseudo-two-phase system whose electron density variation is characterized by

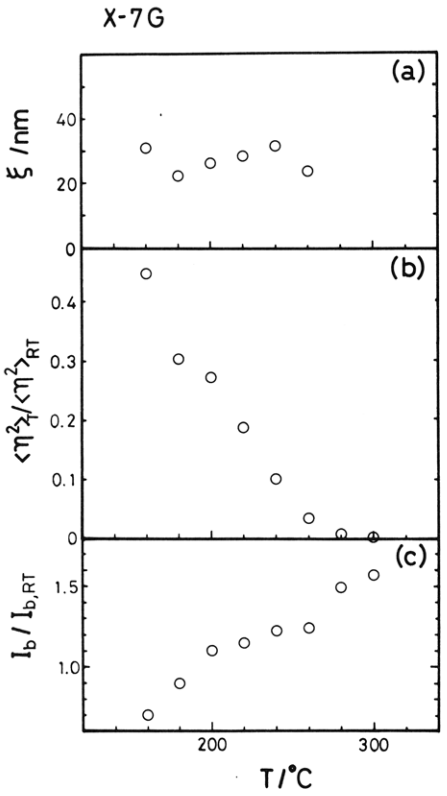

Figure 12. Temperature dependences of (a) Debye correlation length ξ; (b) mean-squared electron density fluctuations relative to that at room temperature, $\langle\eta^2\rangle_T/\langle\eta^2\rangle_{RT}$; and (c) TDS relative to that at room temperature, $I_b/I_{b,RT}$.

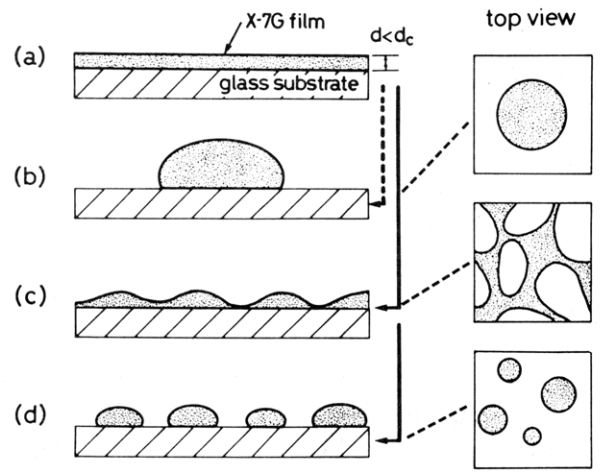

Figure 13. Schematic representations (left, side views; right, top views) of droplet formation from an X-7G thin film ($d < d_c$) due to the unwetting phenomenon. In an ideal case, the final result is (b), but in the actual case the process follows from (a) to (c) and then to (d).

$\rho_{el}(x)$ is given by[36-38]

$$\tilde{I}(s) = I(s)\exp(-4\pi^2\sigma^2 s^2) \tag{8}$$

Thus the Debye plot shows the upward deviation from the straight line in the large s region satisfying $\sigma s \gtrsim 1$. The deviation should be small at $s \ll 1/\sigma$.

Figure 12 shows the temperature dependence of $\xi(T)$ (a), $\langle\eta^2\rangle_T/\langle\eta^2\rangle_{RT}$ (b), and $I_b(T)/I_{b,RT}$ (c). The value $\xi(T)$ was estimated from the Debye plot based upon the scattering profile that was measured in situ at a given temperature T and corrected for $I_b(T)$. $\xi(T)$ is approximately independent of T and 30 nm. The mean-squared electron density fluctuations at T, $\langle\eta^2\rangle_T$, was calculated with $I(0;T)$ estimated from the Debye plot by using the relationship

$$I(0;T) \sim \langle\eta^2\rangle_T \xi(T)^3 \tag{9}$$

where $I(0;T)$ is the zero-scattering vector intensity at T. Since in this experiment we measured only relative intensity, we estimated $\langle\eta^2\rangle_T$ relative to the value at room temperature $\langle\eta^2\rangle_{RT}$. Finally $I_b(t)/I_{b,RT}$ shows the temperature dependence of the TDS relative to that at room temperature $I_{b,RT}$. $\langle\eta^2\rangle_T/\langle\eta^2\rangle_{RT}$ decreases with T as expected. However, it should be noted here that this quantity does not fall to zero even at $T > T_{m,OBA} = 233$ °C, where a significant level of the fluctuations still exist. The TDS level continuously increases with T through the $T_{m,OBA}$ as shown in Figure 12c. There are no discontinuous changes in $\langle\eta^2\rangle_T$ and $I_b(T)$ at $T = T_{m,OBA}$, which may be due to a small crystallinity of X-7G. $I_b(T)$ is expected to increase with T because of increasing isothermal compressibility and decreasing shear modulus and adiabatic compressibility.[39]

IV. A Further Remark: Unwetting Phenomenon

So far we have described the experimental observation on the domain texture and the domain growth for the film specimens with thickness d greater than a certain value d_c. In the case where $d < d_c$, we found a unique pattern due to the unwetting phenomenon in the polarized light micrograph as schematically shown in Figure 13. The as-cast film, which is a glassy amorphous state, has excess surface area and hence excess surface free energy. Thus when it is brought to the liquid-crystal state at $T > T_{m,X\text{-}7G}$, it tends to minimize the surface-to-volume ratio by increasing the thickness and decreasing the surface area as shown in the change from part a to part b in Figure 13. However, in many cases the thickening of the film specimens due to the unwetting effect occurs at many places as shown in part c rather than at a single place as shown in part b. This unwetting process causes the percolated pattern formation as shown in part c, which grows as long as the macroscopic percolation of the liquid crystal can be maintained. The macroscopic percolation eventually breaks to result in the droplets shown in part d. The domain texture as discussed in the preceding sections exists even in the percolated or clustered liquid-crystal domains. The details of this percolation process will be discussed elsewhere.[40] However, our results reported here were obtained for the films with $d > d_c$, hence with uniform film thickness and free from the complication due to unwetting.

V. Conclusion: Model for Thermotropic Liquid-Crystal Texture

We integrate the results obtained by various methods described in section III. The spatial distribution of the disclination lines, most of which have strength of $S = \pm 1/2$, gives characteristic orientation fluctuations of the directors, which give the domain texture under a polarized light microscope (Figures 3 and 4). The correlation length for the orientation fluctuation of directors and hence the average domain size depend on the average number density and spatial configuration of the sign of the disclinations (Figures 4, 5, and 9). The fine striations observed under the TEM are a consequence of the biphasic structure occurring on a few tens of nanometers scale, which resulted from the segregation of the different chemical species into spatially different regions and which was clearly revealed by the SAXS experiments. This biphasic structure was found at temperatures where the X-7G shows a

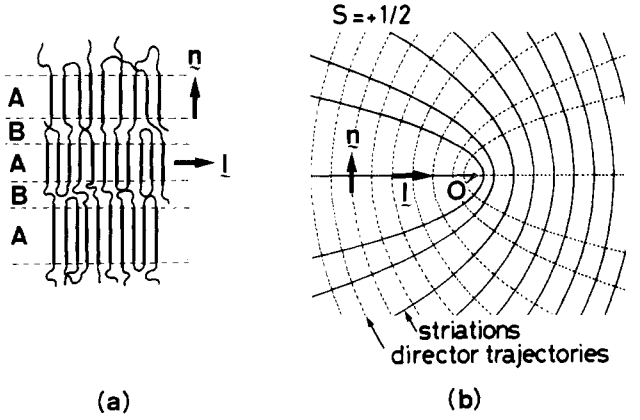

Figure 14. (a) Two-phase model for the microscopic structure of a liquid crystal of X-7G. Regions A consist of relatively rigid segments rich in OBA component, and regions B consist of relatively flexible segments rich in PET component. The difference in density between regions A (high) and B (low) causes the phase contrast in electron microscopy and the scattering of X-rays at small angles. The spacing of alternating layers of A and B is a few tens of nanometers. (b) Relation between the striations observed in the phase-contrast electron micrograph in Figure 8 (solid lines) and the trajectories of directors about the disclination line at 0 ($S = +1/2$). The latter is obtained by rotating the former 180° about 0.

completely anisotropic phase under the optical microscope. Figure 14a shows a schematic model of the liquid crystal on a submicroscopic scale, representing an enlargement of the local structure of the region of circled number thirteen in Figure 9.

In part a of Figure 14 regions A represent those rich in the OBA sequences and hence having higher electron density, while regions B represent those rich in the PET sequences and hence having lower electron density. The segregation of chemically different species of PET and OBA units that are covalently bonded tends to induce inevitably the spatially periodic density fluctuations as shown in Figure 14a, although the model exaggerates the clear periodicity. The periodicity in the real specimen should be less as SAXS profiles of X-7G at higher temperatures exhibit no clear maximum. However, the nature of the periodicity is well manifested by the SAXS for X-7G at 30 °C and by fine striations observed by TEM. The segregation becomes weaker at higher temperatures, as manifested by the decrease of $\langle \eta^2 \rangle$ and by the lowering of the periodicity for the density fluctuations. Yet the segregation exists even at temperatures above the melting point of X-7G.

The striations observed under TEM are a consequence of these density fluctuations, and hence the unit vector parallel to the striation, **l**, is expected to be approximately perpendicular to the director orientation, **n**. Thus the striations shown in Figures 8 and 9 are related to the director trajectories as drawn in Figure 14b where the solid and broken lines indicate the striations and director trajectories, respectively. A single chain traverses regions A and B a number of times, and its global conformation was found to be close to that for a corresponding random coil.[41] This situation is quite reminiscent to the global conformation of a chain in a semicrystalline polymer as expected by the solidification model.[42]

Acknowledgment. We thank Professor H. G. Zachmann for useful discussions. Part of this work was supported by the Japanese Ministry of International Trade and Industry (MITI).

References and Notes

(1) Jackson, W. J.; Kuhfuss, H. F. *J. Polym. Sci., Polym. Chem. Ed.* **1976**, *14*, 2043.
(2) McFarlane, F. E.; Nicely, V. A.; Davis, T. G. In *Contemporary Topics in Polymer Science*; Pearce, E. M., Schaefgen, J. R., Eds.; Plenum Press: New York, 1977; Vol. 2, pp 109.
(3) Acierno, D.; LaMantia, F. P.; Polizzotti, G.; Ciferri, A.; Valenti, B. *Macromolecules* **1982**, *15*, 1455.
(4) Sugiyama, H.; Lewis, D. N.; White, J. L.; Fellers, J. L. *J. Appl. Polym. Sci.* **1985**, *30*, 2329.
(5) Benson, R. S.; Lewis, D. N. *Polym. Commun.* **1987**, *28*, 289.
(6) Mackley, M. R.; Pinaud, F.; Siekmann, G. *Polymer* **1981**, *22*, 437.
(7) Zachariades, A. E.; Economy, J.; Logan, J. A. *J. Appl. Polym. Sci.* **1982**, *27*, 2009.
(8) Mitchell, G. R.; Windle, A. H. *Polymer* **1982**, *23*, 1269.
(9) Viney, C.; Mitchell, G. R.; Windle, A. H. *Polym. Commun.* **1983**, *24*, 145.
(10) Mitchell, G. R.; Windle, A. H. *Polymer* **1983**, *24*, 1513.
(11) Blackwell, J. D.; Lieser, G.; Gutierrez, A. *Macromolecules* **1983**, *16*, 1418.
(12) Joseph, E. G.; Wilkes, G. L.; Baird, D. G. *Polymer* **1985**, *26*, 689.
(13) Joseph, E. G.; Wilkes, G. L.; Baird, D. G. *Polym. Eng. Sci.* **1985**, *25*, 377.
(14) Viney, C.; Donald, A. M.; Windle, A. H. *Polymer* **1985**, *26*, 870.
(15) Shiwaku, T.; Nakai, A.; Hasegawa, H.; Hashimoto, T. *Polym. Commun.* **1987**, *28*, 174.
(16) Lader, H. J.; Krigbaum, W. R. *J. Polym. Sci., Polym. Phys. Ed.* **1979**, *17*, 1661.
(17) Menczel, J.; Wunderlich, B. *J. Polym. Sci., Polym. Phys. Ed.* **1980**, *18*, 1433.
(18) Meesiri, W.; Menczel, J.; Gaur, U.; Wunderlich, B. *J. Polym. Sci., Polym. Phys. Ed.* **1982**, *20*, 719.
(19) Viney, C.; Windle, A. H. *J. Mater. Sci.* **1982**, *17*, 2661.
(20) Nicely, V. A.; Dougherty, J. T.; Renfro, L. W. *Macromolecules* **1987**, *20*, 573.
(21) Nakai, A.; Shiwaku, T.; Hasegawa, H.; Hashimoto, T. *Macromolecules* **1986**, *19*, 3008.
(22) Hashimoto, T.; Suehiro, S.; Shibayama, M.; Saijo, K.; Kawai, H. *Polym. J.* **1981**, *13*, 501.
(23) Todo, A.; Hashimoto, T.; Kawai, H. *J. Appl. Crystallogr.* **1978**, *11*, 558; Todo, A.; PhD Thesis, Kyoto University; Fujimura, M.; Hashimoto, T.; Kawai, H. *Memoirs Fac. Eng., Kyoto Univ.* **1981**, *43*, 224.
(24) Thomas, E. L.; Wood, B. A. *Faraday Discuss. Chem. Soc.* **1985**, *79*, 229.
(25) Economy, J.; Storm, R. S.; Matkovich, V. I.; Cottis, S. G.; Nowak, B. E. *J. Polym. Sci., Polym. Chem. Ed.* **1976**, *14*, 2207.
(26) Frank, F. C. *Discuss. Faraday Soc.* **1958**, *25*, 19.
(27) de Gennes, P.-G. *The Physics of Liquid Crystals*; Clarendon Press: Oxford, 1974.
(28) A different view of the domain will be found in the paper of Wissbrun: Wissbrun, K. F. *Faraday Discuss., Chem. Soc.* **1985**, *79*, 161.
(29) The domain may be defined also as a term that statistically determines the regions where the director orientation is effectively constant. This definition is essentially identical with that given in the text, if there are no domain walls where the director orientation is discontinuous. In both cases the domain is determined by the spatial distribution of the disclinations.
(30) Noel, C. In *Recent Advances in Liquid Crystalline Polymers*; Chapoy, L. L., Ed.; Elsevier Appl. Sci. Pub., 1983.
(31) Friedel, G. *Ann. Phys.* **1922**, *18*, 273.
(32) Kleman, M.; Liebert, L.; Strzelecki, L. *Polymer* **1983**, *24*, 295.
(33) Hashimoto, T.; Nakai, A.; Shiwaku, T.; Hasegawa, H.; Rojstaczer, S.; Stein, R. S. *Macromolecules* **1989**, *22*, 422.
(34) Greco, F. *Macromolecules* **1989**, *22*, 4622.
(35) Debye, P.; Anderson, H. R., Jr.; Brumberger, H. *J. Appl. Phys.* **1957**, *28*, 679.
(36) Ruland, W. *J. Appl. Crystallogr.* **1971**, *4*, 70.
(37) Vonk, C. G. *J. Appl. Crystallogr.* **1973**, *6*, 81.
(38) Hashimoto, T.; Todo, A.; Itoi, H.; Kawai, H. *Macromolecules* **1977**, *10*, 377.
(39) Rathje, J.; Ruland, W. *Colloid Polym. Sci.* **1976**, *254*, 358.
(40) Shiwaku, T.; Nakai, A.; Hasegawa, H.; Hashimoto, T. Unpublished results.
(41) Buchner, S.; Chen, D.; Gehrke, R.; Zachmann, H. G. *Mole Cryst. Liq. Cryst.* **1988**, *155*, 357.
(42) Stamm, M.; Fisher, E. W.; Dettenmaier, M.; Convert, P. *Faraday Discuss. Chem. Soc.* **1979**, *68*, 263.

Registry No. (OBA)(X-7G) (copolymer), 25822-54-2.